Anion exchangers prepared from graft polymerisation of microfibrillated cellulose using the reactive ionic liquid

Muzamil Jalil Ahmed[a], Baohu Wu[b], Antoni Sánchez-Ferrer[a,*]

[a] *Wood Materials Science, Wood Research Institute of Munich (HFM), Technical University of Munich, Munich 80797, Germany*
[b] *Jülich Centre for Neutron Science (JCNS) at Heinz Maier-Leibnitz Zentrum (MLZ), Forschungszentrum Jülich, Garching 85748, Germany*

ARTICLE INFO

Keywords:
Reactive ionic liquids
Glycidyltriethylammonium chloride
Microfibrillated cellulose
Graft polymerisation
Anion exchange

ABSTRACT

Microfibrillated cellulose (MFC) was functionalised using a reactive ionic liquid monomer, *i.e.*, glycidyltriethylammonium chloride (GTEAC), via chain-growth polymerisation, resulting in a novel cationic polyelectrolyte-grafted quaternised MFC (QMFC). The degree of quaternisation and maximum ion exchange capacity of the resulting QMFC were 2.13 mmol/g (*i.e.*, 132 mg/g) and 1.51 mmol/g (*i.e.*, 94 mg/g), respectively. Small-angle X-ray scattering (SAXS) and wide-angle X-ray scattering (WAXS) experiments confirmed the retention of monoclinic crystalline structure for cellulose I with the corresponding decrease in the degree of crystallinity from 85% to 56% and the increase in the spacing between cellulose crystallites by 35%. The presence of the amorphous and grafted polymers was confirmed by microscopy, thermal analysis, and water sorption experiments. QMFC filter cartridges were prepared and tested under dynamic flow conditions with a pressure of 0.2 MPa (retention time of 0.5 min). These cationic polyelectrolytes enhanced multisite ion exchange interactions as evidenced by the Freundlich sorption isotherm. The QMFC filter cartridges demonstrated high anion removal efficiency values of 83.2%, 98.1%, and 94.9% for NO_3^-, SO_4^{2-}, and PO_4^{3-}, respectively. This system achieved a process mass efficiency of 2.79, an *E*-factor of 1.97, and an energy efficiency score of 66.3, which conforms to the green chemistry principles and demonstrates high potential for sustainable water purification.

1. Introduction

Microfibrillated cellulose (MFC) is a versatile, cost-effective, and sustainable material offering a high aspect ratio, excellent mechanical strength, and a large surface area (Lavoine et al., 2012; Xue and Yan, 2024). For separation processes, the use of hydrophilic substrates, such as MFC, allows for greater material permeance to water, which can be controlled by the extent of quaternisation, grafting or cross-linking (Jakubovic and Brook, 1961). This versatility proves vital in modification reactions for applications (Brodin et al., 2017; Ahmed et al., 2024). Quaternised microfibrillated cellulose (QMFC) exhibits increased water compatibility and displays polyelectrolyte behaviour. The final polyelectrolytic fibrous matrix can be easily moulded into nanopapers, beads, sheets, membranes, or filter cartridges, improving versatility and adaptability to different separation systems (Pei et al., 2013; Cheng et al., 2018). A higher degree of quaternisation (*DQ*) implies greater flocculation, gel formulation, or retention of ions by exchange (Song et al., 2008; Kono, 2017). Therefore, QMFC offers more readily accessible functional groups that outperform the performance of the finely ground particles due to its high aspect ratio (Jakubovic and Brook, 1961). The quaternary ammonium $-NR_4^+$ groups have a high

affinity for anions, anionic dyes, proteins, and nucleic acids (Song et al., 2008). Thus, quaternised cellulose can serve as the sustainable, process-adaptive, cost-effective anion exchanger (AEX) that could be used to remove anionic pollutants in commercial or residential wastewater (Pei et al., 2013; Sehaqui et al., 2016). Such anionic pollutants are excess nitrates (NO_3^-), sulphates (SO_4^{2-}) and phosphates (PO_4^{3-}), which are consequences of agro-industrial activity (Waseem et al., 2014; Fida et al., 2022). The excess of these pollutants can lead to hypoxia (O_2 depletion), eutrophication, and mineral imbalance in freshwater bodies.

Early work on the development of cellulosic anion exchangers involved the use of chloroalkylamines, *i.e.*, diethylaminoethyl chloride in aqueous alkaline media (Jakubovic and Brook, 1961). Quaternisation is preferably performed using 3-chloro-2-hydroxypropyltrimethylammonium chloride (CHPTAC) in an alkaline medium that forms the necessary glycidyltrimethylammonium chloride (GTMAC) (Lu et al., 2021; Huang et al., 2022). However, this system can significantly hydrolyse cellulose while intending to disperse it, weakening the material and limiting its performance. This effect can also lead to the decomposition of the GTMAC into enolates (McClure, 1970; Ahmed and Sánchez-Ferrer, 2025). Ionic liquids (ILs), like 1-butyl-3-methylimidazolium chloride ([Bu-MIM]Cl), are used as solvents to disperse cellulose followed by quaternisation using etherifying reagents, while this method allows homogenous cellulose modification and higher degree of substitution, the cost and the total recyclability of ILs remain challenging (Wu et al., 2021). Moreover, the use of such ILs leads to technical and economic complications in the total removal of ILs from the modified MFCs.

A multistep tosylation-based cellulose quaternisation method has also been reported using 1,4-diazabicyclo[2.2.2]octane (DABCO) and diiodobutane. The resulting QMFC had an ionic exchange capacity (*IEC*) in the range of 2.43–3.04 mmol/g. However, the process lacks the advantage of a one-pot, single-step method and incurs the use of multiple reagents and steps to make the anhydroglucose unit (AGU) reactive. This challenge hints at the core issues in cellulose chemistry when modifying with tertiary amines (Schmitt et al., 2011). Alternatively, Mautner et al. (2017) prepared GTMAC-modified cellulosic nanopapers with a *DQ* value of 0.62 mmol/g, and a NO_3^- retention/removal capacity of 1.3 mmol/g (30 g/m^2), compared to the quaternised wood membrane (QWM) L22's 1.07 mmol/g (~42.9 g/m^2) (Ahmed and Sánchez-Ferrer, 2025). Sehaqui et al. (2016) reported mechanochemically modified cellulose nanopapers using GTMAC and alkaline aqueous systems. Shao et al. (2024) reported a GTMAC-based cellulose modification process for the removal of anionic dyes, with a *DQ* or theoretical *IEC* of 1.33 mmol/g. Hassan (2006) reported *Luffa cylindrica* sponge cellulose etherification using diethylaminoethyl chloride. The resulting material absorbed ~2.2 mmol/g of PO_4^{3-}, 2.1 mmol/g of SO_4^{2-}, and 1.9 mmol/g of NO_3^- over 2 h. Bottle gourd (*Lagenaria vulgaris)* shells have been quaternised using GTMAC, yielding a quaternised biosorbent with a PO_4^{3-} removal of 1.12 mmol/g over 1 h (Marković-Nikolić et al., 2018).

In earlier work, we have demonstrated a direct, cost-effective anhydrous Menshutkin reaction for preparing a polymerisable, glycidyl reactive IL (RIL), *i.e.*, glycidyltriethylammonium chloride (GTEAC) (Ahmed and Sánchez-Ferrer, 2025). Moreover, based on a model study in our earlier work, we demonstrated the chain-growth polymerisation of this GTEAC monomer. This feature leads to long cationic polyelectrolytes with a high degree of polymerizasion which can reduce ion migration, thereby increasing contact time and instances of multi-layer homovalent ion exchange or partial chemisorptive interactions (Freundlich ion exchange/absorption) (Sata, 2004). The use of GTEAC offers a higher hydrophilic effect than trimethylammonium (Koga et al., 2013), and greater overlapped regions that can undergo ion exchange.

The present work intends to utilize the GTEAC's tendency to polymerize to form long-chain polyelectrolytic grafts, to increase the IEC of the modified MFC. The polymerisation of ILs is well-known for imidazolium, pyridinium, and pyrrolidinium monomers yielding long-chain cationic polyelectrolytes (Eftekhari and Saito, 2017). However, to our knowledge, chain-growth polymerisation using RILs, such as GTEAC, and their grafting onto cellulose surfaces is scarcely reported.

The present work investigated further use of GTEAC polymerisation with MFC to develop novel cationic polyelectrolyte-grafted QMFCs. The polyelectrolytic behaviour and ion exchange properties of the GTEAC-based QMFCs were investigated. Moreover, these AEXs have been used in a simple dead-end filter cartridge system to study their removal efficiencies against NO_3^-, SO_4^{2-}, and PO_4^{3-}. The filter cartridge system was used to determine its applicability in small scale or lab scale, portable applications to obtain ultra-deionised water. The performance of the QMFCs with those produced by common aqueous alkaline etherification systems was further compared based on chloralkylamines and CHPTAC or GTMAC, and against similar lignocellulosic AEXs and wood AEXs. The QMFC preparation has also been assessed using certain metrics corresponding to the green chemistry principles (DeVierno Kreuder et al., 2017).

2. Materials and methods

2.1. Materials

Celova® C500 cellulose powder (length: 0.5–1.6 mm; 32 μm accounting for 60%–75%) was provided by Weidmann Fiber Technology AG (Switzerland). Epichlorohydrin (99%) and triethylamine (99.7%) bought from ThermoFisher Scientific (Germany) and Sigma-Aldrich (Germany), respectively, were used as received for the GTEAC synthesis. Sodium hydroxide (NaOH), sodium chloride (NaCl), sodium nitrate ($NaNO_3$), sodium sulphate (Na_2SO_4), disodium hydrogen phosphate (Na_2HPO_4), and all other ancillary chemicals were procured from Merck kGaA (Germany). Deuterium oxide (D_2O) with the deuterium content of 99.9% was acquired from VWR Avantor (Germany). Deionised water was used for the oxoanion removal experiments, while all other analysis used ultra-deionised MilliQ Type 1 water (conductivity: 0.055 μS/cm). Feed solutions based on NO_3^- and SO_4^{2-} were at pH = 7 except PO_4^{3-} feeds which were at pH > 12 (pK_a = 12.4, *i.e.*, 50% HPO_4^{2-} and PO_4^{3-}).

2.2. Methods

2.2.1. The GTEAC synthesis

The GTEAC was synthesized and characterised according to the procedure described in an earlier work by Ahmed and Sánchez-Ferrer (2025). Details regarding a model polymerisation study of GTEAC with an *n*-butanol initiator (imitative of the cellulose AGU) were also described therein. The purity of the GTEAC was 94% (according to ^{1}H NMR analysis).

2.2.2. Quaternised microfibrillated cellulose preparation

The MFC quaternisation was performed with GTEAC using a previous method (Ahmed and Sánchez-Ferrer, 2025). Briefly, MFC was dried for ~1.5 h at 110 °C in an air-convection oven (Memmert, Germany) until a constant dry weight was obtained. Then 5 g (corresponding to 30.84 mmol of AGU) of the dried MFC was transferred to a reaction vessel, *i.e.*, an air-tight glass container. The 58.6 g (370.1 mmol) GTEAC was carefully added, and the resulting mixture was kneaded manually for 5 min. The kneading was performed until all fibrous materials were well-mixed, after which the container was kept under N_2 atmosphere for 2 min and sealed. The reaction container was then placed in a convection oven for 1.5 h at 90 °C. Partially-reacted MFC was kneaded again for 5 min, the reaction vessel was made inert and sealed for further reaction for 0.5 h. The GTEAC and the MFC (*i.e.*, AGU unit) were reacted in a 12:1 molar ratio. It is worth mentioning that for this reaction, the GTEAC monomer can decompose into a water-soluble decomposate oil (quaternary enolates) as previously observed by Ahmed and Sánchez-Ferrer (2025). Thus, the resulting QMFC was then washed several times with deionised water to remove excess reactant and decomposates until a clear filtrate was obtained. The QMFCs were dried for 1.5 h at 80 °C.

The weight gain (w_g) and the degree of quaternisation (DQ) were calculated referring to the original MFC dry mass as shown in Eqs. (1) and (2):

$$w_g = \frac{w - w_0}{w_0} \times 100\% \tag{1}$$

$$DQ = \frac{w - w_0}{w_0 \, M_{GTEAC}} \tag{2}$$

where w_0 and w are the dry mass of the MFC and the QMFC, respectively, and M_{GTEAC} is the molar mass of the GTEAC ($C_9H_{20}NOCl$: 193.72 g/mol). The theoretical or maximum *IEC* when given by the same degree of quaternisation is defined as $IEC_{0,max}$. However, it is more practical to relate this parameter to the total composition of the QMFC (*i.e.*, MFC + poly-GTEAC), as the maximum of ionic exchange capacity (IEC_{max}) equals to degree of quaternisation multiplied by w_0/w.

2.2.3. Fourier transform infrared spectroscopy

Fourier transform infrared (FT-IR) spectroscopy was recorded using a Nicolet iS50 (ThermoFisher Scientific, USA) spectrophotometer with an attenuated total reflectance (ATR) accessory (diamond/ZnSe crystal). Spectra were recorded in the range of 4000–500 cm^{-1} and measured at a spectral resolution of 4 cm^{-1} and averaged over 64 scans. The FT-IR experiments with D_2O-masking were conducted to ascertain spectral peaks related to the QMFC and MFC other than those of absorbed water. Briefly, 20 mg sample was soaked in D_2O for 24 h, then dried in a desiccator for another 24 h before the FT-IR was measured.

2.2.4. Thermal characterization

Thermogravimetric analysis (TGA) experiments were performed using a TGA50/M3 from Mettler Toledo (Switzerland) and controlled by a TC15 TA controller Mettler Toledo (Switzerland). 5 mg sample were placed in 70 µL aluminum oxide standard capsules. The TGA was conducted from 25 to 1000 °C at a heating rate of 10 K/min under an inert atmosphere. Differential scanning calorimetry (DSC) experiments were carried out on a DSC 822 (Mettler Toledo, Switzerland) calorimeter with an autosampler. 5 mg sample were placed in a 40 µL perforated aluminum pan. The DSC was taken from –50 °C to 500 °C at a heating rate of 10 K/min under an inert atmosphere.

2.2.5. Scanning electron microscopy/energy-dispersive x-ray analysis

Scanning electron microscopy (SEM) images were captured using a Carl Zeiss EVO-40 XVP (Carl Zeiss, Germany) electron microscope to examine the microstructure of MFC and QMFC. Energy-dispersive X-ray (EDX) analysis was also performed to identify the presence of the different atoms in the sample. Operating conditions for the EDX were in low vacuum (~0.01 Pa) with an accelerating voltage of 15 kV at 97× magnification. Fibre size dimension analysis was conducted using ImageJ, and non-linear curve fittings were performed using a generalised extreme value (GEV) distribution.

2.2.6. X-ray characterisation

Small-angle X-ray scattering (SAXS) and wide-angle X-ray scattering (WAXS) experiments were performed using a XUESS 3.0 XL KWS-X (Xenocs, France) equipped with a high flux Metal-Jet D2+ X-ray source (Excillum, Sweden) featuring a liquid metal anode (250 W; 70 kV; 3.57 mA) with $\lambda_{GaK\alpha}$ radiation wavelength of 0.1314 nm to obtain direct information on the scattering patterns. The X-ray scattered intensity was collected using a 2D Eiger2R 4M (Dectris, Switzerland) X-ray detector (15.5 cm width × 16.3 cm height; 75 µm resolution) with a sample-to-detector distance from 0.1 m to 1.70 m An effective scattering vector range of 0.05 $nm^{-1} < q < 45$ nm^{-1} was obtained, where q is the scattering wave vector ($q = 4\pi \sin\theta / \lambda$). The degree of crystallinity (χ) was

calculated by the deconvolution of the WAXS signal into crystalline and amorphous peaks in the WAXS patterns, the areas of which give the $\chi = A_{\text{crystalline peaks}} / (A_{\text{crystalline peaks}} + A_{\text{amorphous peaks}})$ (Arcari et al., 2019; Bertsch et al., 2019; Scheuchzer et al., 2022; Engelhardt et al., 2024). The SAXS intensity profiles were fitted using a pseudo-Voigt peak function that allowed for the evaluation of the scatterers' distance (D) and the correlation length (ξ).

2.2.7. Dynamic vapour sorption

Dynamic vapor sorption (DVS) experiments were conducted as described by Sánchez-Ferrer et al. (2023), using a gravimetric DVS Advantage ET (Surface Measurement Systems, UK) vapor sorption device. The device comprises a microbalance and an N_2-purged chamber with a 200 cm^3/min (12 L/h) flow at a selected relative humidity (RH). Samples were initially conditioned at 25 °C and 0% RH until completely dry. Measurement starts with the increase in RH of the N_2 flow in steps of 5% until ~100% RH (adsorption). The RH is cycled back (desorption), reducing in steps of 5% until 0% RH. The criterion for change in RH is related to slope of the water mass uptake during the sorption process (lower than 0.001%/min over 10 min), at this point, the sample is measured for one extra hour before changing the RH for the next measuring step. Each dynamic moisture sorption step was analyzed using a double stretched exponential (DSE) model (Sánchez-Ferrer and Engelhardt, 2025), and the extrapolated values were used to construct the corresponding moisture sorption isotherms and fitted using the modified Guggenheim, Anderson, and de Boer (GAB) model (Berthold et al., 1996; Viollaz and Rovedo, 1999). The sorption site occupancy (SSO) model was implemented to evaluate the number of binding sites per mass of the sample (Willems, 2014; 2015).

2.2.8. Oxoanion removal performance

Filter cartridges were prepared as shown in Fig. S1 with specific QMFC packing concentration (PC, w/V) and bed volume (BV, mL). These column parameters were varied to study the oxoanion removal/ion exchange performance. The PC and BV values are interrelated and given by the following relation: $PC = w_p / BV \times 100\%$, where w_p corresponds to the packing mass (g). Briefly, dried QMFC was first slurried with a 1 mol/L NaCl solution to 24.7%–27.2% (w/V) packing concentration corresponding to BV values of 5.9 mL (height of the cylinder, h = 13.5 mm) and 14.96 mL (h = 34.5 mm), respectively. The slurry was stored for at least 24 h (pre-conditioning) and then compressed into a specific cylindrical stainless steel mould. The QMFC packing was then sandwiched between two Whatman 21 cellulose filter papers (23.5 mm diameter, 0.1 mm thick). The filter packing was washed with MilliQ water several times to remove excess Cl^- and inserted into the filter cartridge system. A 24.7% (w/V) MFC packing (BV: 14.96 mL, h = 34.5 mm) was also prepared in a similar method to compare performances.

The ultrafiltration/ion exchange dead-end filter cartridge system was retrofitted from a 500 mL portable/outdoor water filter system (185 mm length × 30 mm outside diameter; 23.5 mm inside diameter) acquired from Gavgroom (China). This assembly (Fig. S1a) was used to test the QMFC and MFC oxoanion removal performance (η_i), where i corresponds to unitary oxoanion feedstocks (*i.e.*, NO_3^-, SO_4^{2-}, and PO_4^{3-}). All feed solution concentrations were ~45 mg/L (pH = 7) and 50 mg/L (pH = 7), except for PO_4^{3-} feeds: 2.4 mg/L (pH = 12). The dead-end filtration/ion exchange was performed using an in-built diaphragm pump (Fig. S1b), allowing for a constant flow rate of 98.3 mL/min under a pumping pressure < 0.2 MPa. The η_i was calculated as Eq. (3):

$$\eta_i = \left(1 - \frac{n_{p,i}}{n_{f,i}}\right) \times 100\% \tag{3}$$

where $n_{f,i}$ and $n_{p,i}$ refer to the moles of oxoanion i (*i.e.*, NO_3^-, SO_4^{2-}, PO_4^{3-}) removed for the feed and the permeate, respectively. The NO_3^-, SO_4^{2-}, and PO_4^{3-} concentrations were determined using the spectrophotometric methods described by Ahmed and Sánchez-Ferrer (2025). All measurements were performed in ambient conditions. The retention of the exchanged oxoanions (*i.e.*, stability) was also studied through repetitive filtration experiments using the same filter cartridge (between QMFC and MFC). It is worth noting that the terms oxoanion removal and retention have been used interchangeably, equivalent to chemisorption.

The performance of the QMFC and MFC in the filter cartridge assembly was further studied using the penetration depth (L_i). The penetration depth for an oxoanion i (*i.e.*, NO_3^-, SO_4^{2-}, and PO_4^{3-}) is given by Eq. (4):

$$\eta_i = 1 - e^{-h / L_i} \tag{4}$$

where h = 34.5 mm (QMFC) and 38.9 mm (MFC) for the same packing concentration, *i.e.*, 24.7% (w/V); η_i is the oxoanion removal/ion exchange.

2.2.9. Ion exchange capacity

The ion exchange capacity (*IEC*) corresponds to the amount of charged functional groups per mass of the dry ion exchanger. The *IEC* of the QMFC was spectrophotometrically determined using the Cd-reduction method described by Ahmed and Sánchez-Ferrer (2025). The method correlates the NO_3^- concentration with the absorption intensities of the reagent. A HI97728 nitrate photometer (≤ 130 mg/L NO_3^- range, ±0.5 mg/L accuracy, λ = 425 nm) acquired from Hanna Instruments (Romania) was used. The *IEC* under flow conditions can be estimated using Eq. (5):

$$\text{IEC} = \frac{n_f - n_p}{w} \tag{5}$$

where n_f and n_p correspond to the number of moles of NO_3^- in the feed and permeate, respectively. The apparent IEC under equilibrium was also determined. Briefly, 100 mg pre-charged QMFC fibres were soaked in 10 mL $NaNO_3$ (1 mol/L) for 48 h. The QMFCs were

filtered and washed several times with MilliQ water, then immersed in a 0.5 mol/L aqueous NaCl solution. The apparent IEC (in mmol/g NO_3^-) under zero flow can be calculated by Eq. (6):

$$\mathrm{IEC} = \frac{C_{NO_3} V_{NO_3}}{w M_{NO_3}} \tag{6}$$

where C_{NO_3}, V_{NO_3}, and M_{NO_3} are the concentration, volume, and molar mass of the NO_3^- ion (62 g/mol), respectively; w is retained QMFC mass. The theoretical ion exchange capacity ($IEC_{0,max}$) based on the QMFC weight is given as: $IEC_{0,max} = IEC_{max} \times w/w_0$. Alternatively, the interchangeable parameter, absorption capacity (AC, mg per 1 g of NO_3^-) is given as: $AC = IEC \times M_{NO_3}$.

2.2.10. Equilibrium and flow ion exchange studies

An isothermal experiment for the QMFC was performed to study the ion exchange behavior. The NO_3^- concentrations are in the range of 10^{-5}–10^{-3} g/g (0.3–20 mmol/L). The ion exchange data was modelled using a Freundlich isotherm that accounts for a multilayer ion-surface interaction, which is likely to be the case with multi-ion/interface (polyelectrolytic) interactions (Azizian and Eris, 2021). The Freundlich isotherm assumes that for a finite IEC_{max}: (1) heterogeneous adsorption sites/surfaces; (2) multilayer absorption/ion exchange; (3) equilibrium between ions in solution and ions exchanged; (4) ion exchange independence (*i.e.*, one ion for one binding group); and (5) non-ideal ion exchange occurs, given by an exponential factor (a), where $0 \leq a \leq 1$ (Wang and Guo, 2020). The Freundlich isotherm for an apparent *IEC* can be given as Eq. (7):

$$IEC = IEC_{max} (K\ C)^a \tag{7}$$

where, K, C, and a are the ion exchange constant at equilibrium, the ionic concentration at equilibrium, and the non-linear exponential factor, respectively.

However, the oxoanion retention/release is more practical when considering the exchanged anions with respect to the total number of cationic sites; therefore, using the difference in the number of moles of oxoanion exchanged (Δn), the calculation results are independent of the mass of the filtering material. Thus, the modified Freundlich relation is given as Eq. (8) (Misak, 1993; Wang and Guo, 2020):

$$\Delta n = \Delta n_{max} (K\ C)^a \tag{8}$$

where Δn_{max} is the maximum number of moles of the exchanged oxoanion.

2.2.11. Green chemistry indicators

DeVierno Kreuder et al. (2017) proposed a process-specific Green Chemistry Metrics assessment which quantifies the progress of process, synthesis or materials in terms of the 12 green chemistry principles given by the Anastas and Warner (2000). To ascertain the techno-economic and sustainability of our QMFC preparation method, we focused on selected process-specific parameters, such as:

(1) Atom economy, defined by the process mass efficiency (*PME*) as shown in Eq. (9):

$$PME = \frac{m_{\text{reactant}} + m_{\text{auxiliary chemicals}} - m_{\text{recovered reactant}} - m_{\text{recovered auxiliary chemicals}}}{m_p + m_{cp}} \tag{9}$$

where, m_p and m_{cp} are the mass of the product and the co-product formed, respectively.

(2) Less hazardous chemical synthesis (*HCS*) defined by Eq. (10):

$$HCS = \frac{\sum_{i=1}^{n} H_i\ m_{rm,i}}{m_p} \tag{10}$$

where, H_i is hazard score estimated for each raw material i, which is based on the Global Harmonised System of Classification and Labelling of Chemicals; $m_{rm,i}$ is the mass of raw material i. The estimation of the H_i is defined by an exposure score tabulated and briefly described by DeVierno Kreuder et al. (2017).

(3) Energy efficiency (*EE*) is given as Eq. (11):

$$EE = \frac{\sum_{i=1}^{n} \left[t\ m_{rm} \left(F_{T,i} + F_{P,i}\right)\right]}{m_p} \tag{11}$$

where, m_{rm} is the mass of raw materials; t is time; $F_{T,i}$ and $F_{P,i}$ are temperature and pressure severity factors, respectively.

The *PME* parameter focuses on efficient input use (resource efficiency) according to NSF/GCI/ANSI 355–2011 (Greener Chemical and Processes Information, USA). The *EE* parameter calculates the energy impact in chemical production by calculating reaction time deviation from ambient pressure and temperature, addressing the lack of commonly measured energy usage (DeVierno Kreuder et al., 2017). Details regarding the selection of the appropriate temperature and pressure severity factors for a time (t) are reported extensively by DeVierno Kreuder et al. (2017). The *E*-factor, which is the ratio of waste or co-product to the product produced, has also been determined by $E = m_{cp}/m_p$ (Sheldon, 2018).

3. Results and discussion

3.1. Preparation and characterisation of QMFC

The QMFC preparation followed a similar quaternisation reaction reported in the earlier work, using pinewood scaffolds (Ahmed and Sánchez-Ferrer, 2025). The MFC quaternisation targets all three OH groups in the amorphous domains or the crystallite surface of cellulose as shown in Fig. 1. The quaternisation reaction is ramped up at higher temperatures, *i.e.*, 90 °C, as reactions at low temperatures yield insubstantial results (Song et al., 2008). The quaternisation time was increased to 2 h to facilitate the formation of the cationic polyelectrolytes, *i.e.*, poly-GTEAC. It is necessary to maintain an anhydrous atmosphere throughout the reaction to prevent the RIL degradation, as observed elsewhere (Song et al., 2008; Sehaqui et al., 2016; Mautner et al., 2017; Ahmed and Sánchez-Ferrer, 2025).

A mol ratio of 12:1 between the GTEAC and MFC was used since it allowed for optimal mixing of the two components. The quaternisation reaction leads to a weight gain (w_g) of 41.39% corresponding to a *DQ* of 2.13 mmol/g, similar to that for quaternised wood (owing to reaction time) (Ahmed and Sánchez-Ferrer, 2025). Higher reaction times (> 2 h) were limited by the decomposition of the GTEAC at 90 °C. Attempts with lower molar ratios (*i.e.*, GTAC:MFC = 3.0 or 7.5) were also conducted, though the resulting fibres had poorer mixing and low conversion. The reaction conditions were optimized at 90 °C for 2 h based on the results of the GTEAC polymerisation in the model study reported by Ahmed and Sánchez-Ferrer, 2025. The high number of polyelectrolytes leads to unstable aqueous dispersions where an aggregating effect and floc formation occur, making NMR experiments with the QMFC impractical. Nevertheless, as shown in Fig. 2, the ATR-FTIR spectrum showed the obvious peaks of QMFC: 3 309 (st, C–OH), 3290 (st, –CH_3), 2882 (st, –CH–), 1631 (st, absorbed H_2O), 1473 (st, C–N (poly-GTEAC)), 1426–1321 (δ, –CH (AGU)), 1374 (δ, geminal CH_2), 1095–1153 (st, C–O), 1023–1055 (st, C–O–C), 850 cm^{-1} (δ, C–H), and demonstrated successful MFC quaternisation based on

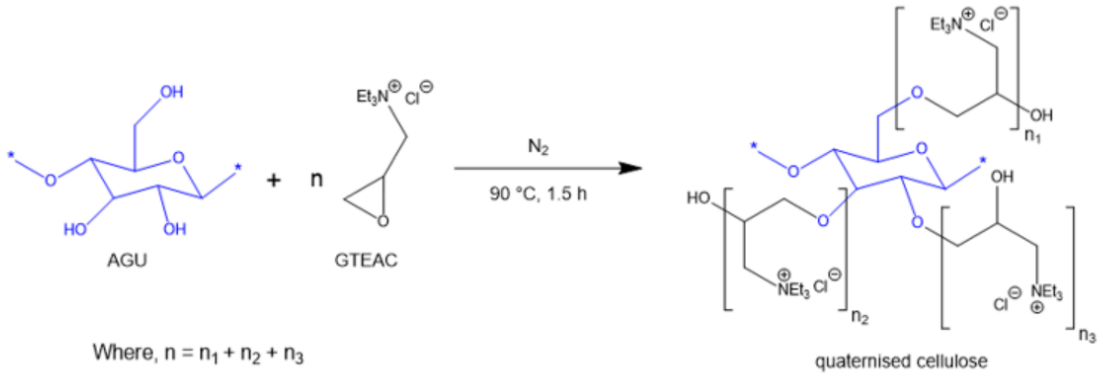

Fig. 1. Reaction scheme for microfibrillated cellulose quaternisation. Adapted from Ahmed and Sánchez-Ferrer (2025), published by Elsevier B.V., under Creative Commons CC-BY 4.0 license.

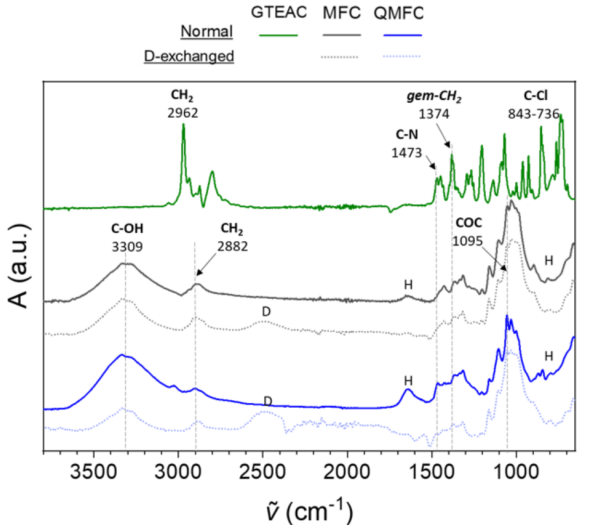

Fig. 2. Attenuated total reflectance-Fourier transform infrared (ATR-FTIR) spectra for glycidyltriethylammonium chloride (GTEAC), microfibrillated cellulose (MFC), and quaternised microfibrillated cellulose (QMFC) with and without D_2O-labelling (GTEAC not shown).

the characteristic $-NEt_3^+$ peak at 1473 cm^{-1}. The D_2O-labelled FT-IR spectrum also indicated interactions due to absorbed water (*e.g.*, 1631 cm^{-1}), which were evidently higher for the QMFC as it is more hydrophilic than the MFC. The absorption profile for the cellulose chain remained practically the same other than the D_2O peak at ~2500 cm^{-1} and $-NEt_3^+$ peak at 1473 cm^{-1}.

3.2. Structural and morphological properties

SEM experiments were performed to observe the surface and morphological features of the neat MFC and the QMFC (Fig. 3). The effect of the grafted polymers is evident in the QMFC sample, where individual fibril bundles appear to have a more distinct roughness, waxy appearance, indicating coverage by amorphous material(s), *i.e.*, the poly-GTEAC. The SEM micrographs for QMFC showed the development of the so-called floc (entangled) structures. It is likely that a network of cationic polyelectrolytic microfibrils and larger expanded fibrillar aggregates are formed (Kopač et al., 2022). This implies that there are indeed numerous entangled amorphous polyelectrolytic domains in the QMFC which could contribute to enhanced ionic interactions.

The MFC appeared as fibre bands with an average width of (27.1 ± 9.2) μm and an average thickness of (2.9 ± 1.4) μm, and the QMFC had a thickness of (6.7 ± 1.7) μm while keeping almost the same width of (27.5 ± 8.4) μm. This corresponds to a two-fold increase in the thickness based on the size distribution analysis in Fig. S2. Fibril lengths can be affected by the aqueous alkaline CHPTAC or GTMAC quaternisation processes which can cause cellulose chain scission in the amorphous domains (*i.e.*, mercerisation or hydrolysis) (Gupta et al., 2013; Pei et al., 2013). However, this is not the case with the present work, as the QMFC quaternisation was conducted in the absence of alkaline media. This helped preserve the natural structure of the MFC and allowed for adequate modification of the cellulose units exposed to the reactive GTEAC.

The EDX experiments were also performed to determine the elemental analysis of the samples and to ascertain qualitatively the presence of N from the quaternary ammonium (NEt_3^+) groups and Cl as the counter-ions from the grafted poly-GTEAC. As shown in Fig. 3a, only C and O were present in MFC due to the detection of the corresponding kα emission lines at 0.277 and 0.525 keV, respectively. The EDX analysis of QMFC also evidenced the presence of N and Cl from the $\kappa\alpha$ emission line at 0.392 keV (N), and the $\kappa\alpha$ and $\kappa\beta$ emission lines at 2.622 and 2.816 keV (Cl), respectively (Fig. 3b), meanwhile, the peaks at 1.487, 1.041, and 1.740 keV corresponded to impurities related to Al, Na, and Si.

WAXS and SAXS experiments were performed to determine any structural change in the cellulose crystalline domains as well as any change in the assembly of these crystallites. Figs. 4a and b show the WAXS analysis of both MFC and QMFC revealing that the

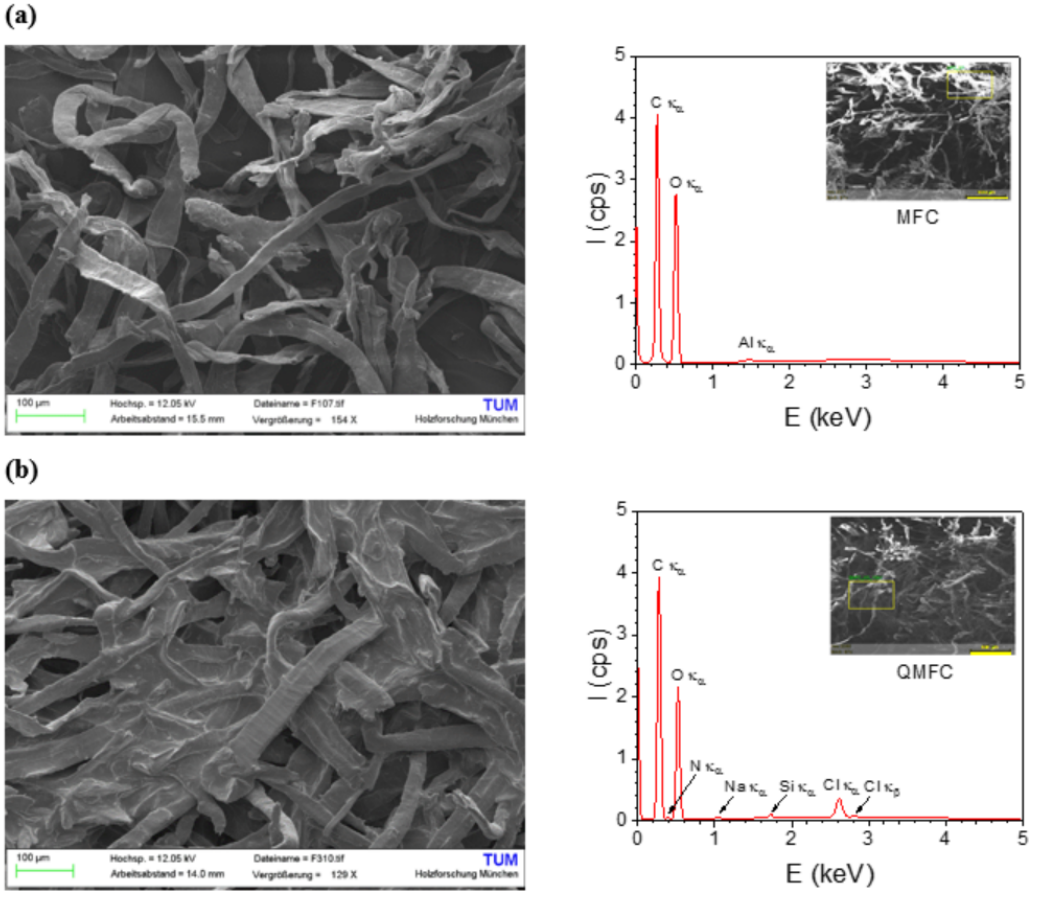

Fig. 3. Scanning electron microscopy (SEM) micrographs and the corresponding energy-dispersive X-ray (EDX) analysis for (a) MFC and (b) QMFC.

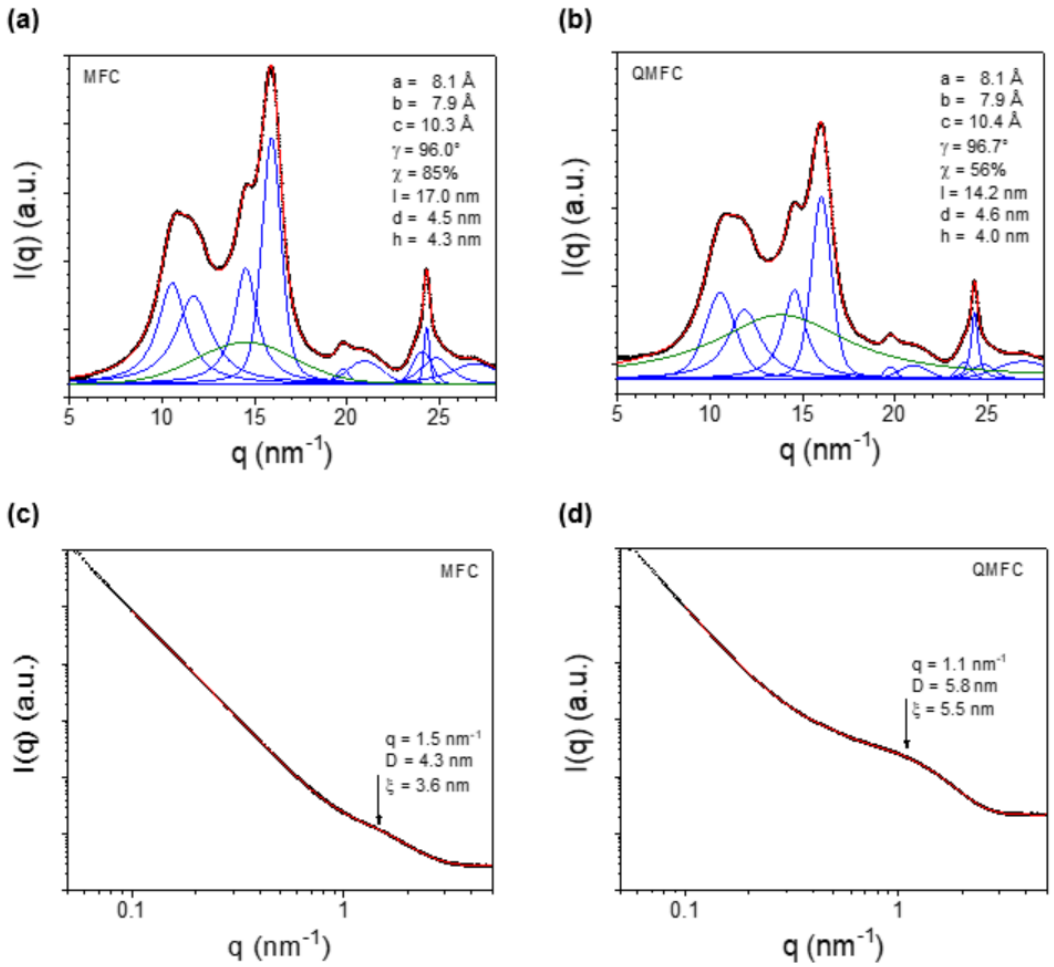

Fig. 4. The wide-angle X-ray scattering (WAXS) profile for (a) MFC and (b) QMFC together with the corresponding lattice parameters (*a, b, c*, and γ), degree of crystallinity (χ), and the average length (l), width (d), and thickness (h) of the cellulose single crystal; The small-angle X-ray scattering (SAXS) profile for (c) MFC and (d) QMFC and the corresponding lateral average distance (D) between cellulose single crystals with the corresponding correlation length (ξ) between these crystalline domains.

grafting process does not alter the original cellulose's crystalline domains, *i.e.*, monoclinic cellulose I allomorph, keeping constant the lattice parameters (a = 0.81 nm, b = 0.79 nm, c = 1.03 nm, and γ = 96.0°). Moreover, from the shape of the crystalline peaks (blue curves), the average length (l), width (d) and thickness (h) of the cellulose crystallites were determined (l = 17 nm, d = 4.5 nm, and h = 4.2 nm), which remained almost constant after the grafting process. Finally, the degree of crystallinity was determined for both samples by the ratio between the area of all crystalline peaks (blue curves) with respect to the total area of the scattering signal (red curve). The results indicated a decrease in the degree of crystallinity (χ) from 85% to 56% after grafting, showing that amorphous material were incorporated into the structure. The degree of crystallinity for the QMFC (χ_{QMFC}) was predicted from the mass gain (w_g) and the degree of crystallinity (χ_{MFC}) of the MFC sample, *i.e.*, $\chi_{QMFC} = \chi_{MFC}\ (1 - w_g\ /\ (1 + w_g))$. The theoretical value was 60% which was very close to the measured value by the WAXS analysis of 56%. SAXS experiments (Figs. 4c and d) indicated an increase in the lateral distance between the crystalline domains as observed by the shift of the broad peak (q) from 1.5 nm^{-1} to 1.1 nm^{-1}. This shift corresponded to an increase (35%) in the average lateral distance (D) from 4.3 nm (MFC) to 5.8 nm (QMFC) after grafting, indicating that poly-GTEAC occupies some space between the cellulose single crystals. Moreover, the correlation length (ξ) between these crystallites is 3.6–5.5 nm, showing the random distribution of the cellulose single crystals within the amorphous matrix. All the parameter values from the WAXS and SAXS analysis were summarised in Table 1.

3.3. Thermal properties

The thermal characterisation of the QMFC further elaborates the impact of the inclusion of amorphous cationic polyelectrolytes, *i.e.*, poly-GTEAC, on the MFC fibril surface. Figs. 5a and b show the TGA and the derivative thermogravimetry (DTG) analysis, respectively, of the MFC and QMFC samples. There was an apparent decrease in the decomposition temperature from 355 °C (MFC) to 340 °C (QMFC), corresponding to the native cellulose chains (Li et al., 2024). The deconvolution of the DTG signal for the QMFC

Table 1
Lattice parameters (*a, b, c*, and γ), degree of crystallinity (χ), the average dimensions of the cellulose single crystal (*l, d*, and *h*), and the lateral distance between crystallites (*D*).

Item	*a* (nm)	*b* (nm)	*c* (nm)	γ (°)	χ (%)	*l* (nm)	*d* (nm)	*h* (nm)	*D* (nm)
MFC	0.81	0.79	1.03	96.0	85	17.0	4.5	4.3	4.3
QMFC	0.81	0.79	1.04	96.7	56	14.2	4.6	4.0	5.8

Notes: MFC, microfibrillated cellulose; QMFC, quaternised microfibrillated cellulose.

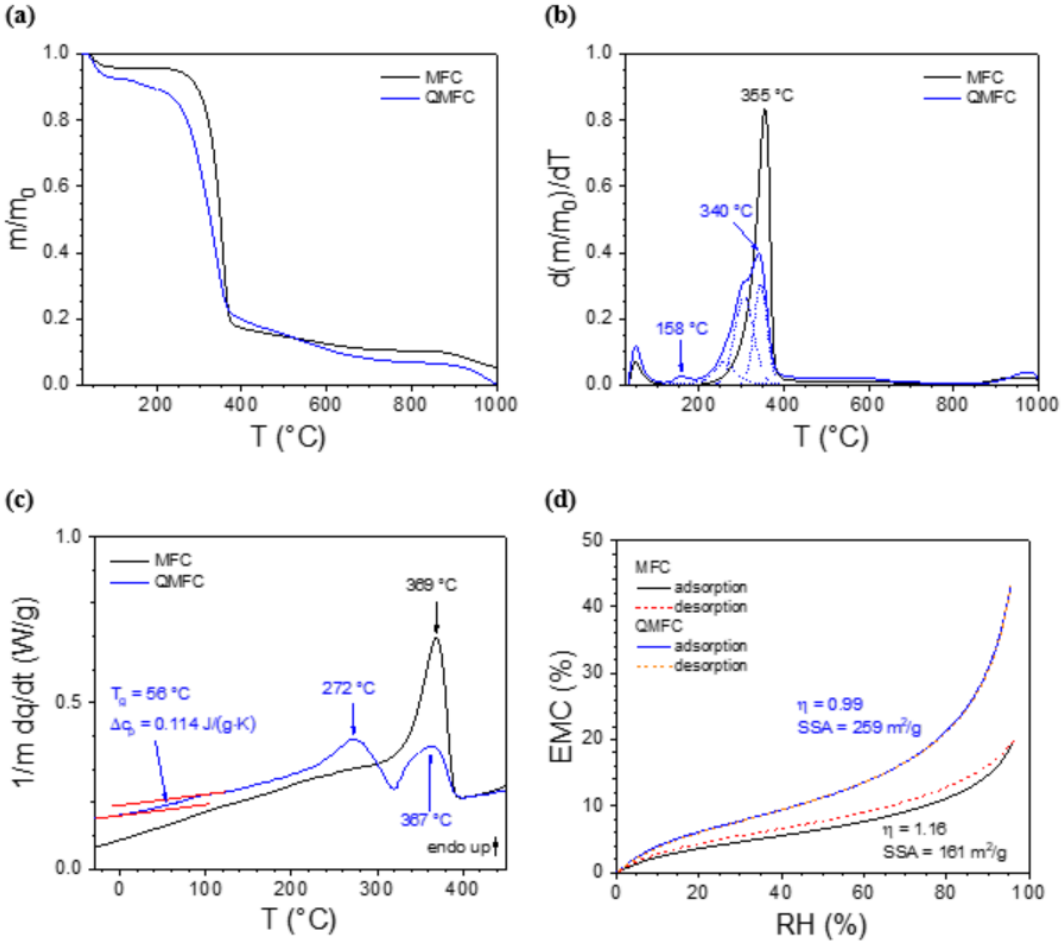

Fig. 5. (a) Thermogravimetric analysis (TGA) thermograms, (b) the corresponding TGA thermogram derivatives, and (c) the DSC thermogram for MFC and QMFC; (d) Vapour adsorption/desorption isotherms for both the MFC and the QMFC with the corresponding specific surface area (SSA) and the hysteresis coefficient estimated using the modified Guggenheim, Anderson, and de Boer (GAB) model.

showed three peaks at 260, 306, and 345 °C, where the first peak can be associated with the model poly-GTEAC at 223 °C (Ahmed and Sánchez-Ferrer, 2025). The grafted poly-GTEAC had a higher decomposition temperature owing to its high degree of polymerisation (*DP*) compared to that of the model polymer (*DP* = 13). The tiny peak at 158 °C could be attributed to some residual grafted oligosaccharides or impurities.

Fig. 5c shows the DSC thermograms of both fibrous materials. The MFC only showed a huge endothermic peak corresponding to cellulose decomposition, which occurred at 369 °C for the MFC, similar to that described by Li et al. (2024). Contrary to that, QMFC clearly showed a glass transition temperature (T_g) at 56 °C (change in heat capacity (Δc_p) = 0.114 J/(g•K)) for the QMFC. This value is in between the one from the model poly-GTEAC (T_g = 8 °C, Δc_p = 0.350 J/(g•K)) and from quaternised pinewood membrane (T_g = 90 °C, Δc_p = 0.120 J/(g•K)) (Ahmed and Sánchez-Ferrer, 2025). This increase in the glass transition temperature with respect to the model poly-GTEAC implies the attachment of the grafted polymer to more rigid substrates (MFC fibrils and lignocellulosic scaffolds). Additionally, a two-step thermal decomposition was observed for QMFC where the amorphous component (*i.e.*, the poly-GTEAC) decomposed at ~272 °C and the cellulose component decomposed at 367 °C, which quite matched the values observed in Fig. 5c. Moreover, from the increase in the heat capacity of the QMFC sample (Δc_p = 0.114 J/(g•K)) and compared to the value

Table 2
Summary of process input parameters, such as flow velocity (u_v), and hydrodynamic retention time (t_{ret}) and the resulting removal performance ($\eta_{NO_3^-}$, $\eta_{SO_4^{2-}}$, and $\eta_{PO_4^{3-}}$).

Item	MFC		QMFC	
Bed volume (BV, mL)	5.86[a]	14.86[b]	5.86	14.86
Filter loading (FL, mL/mL)[c]	17.06	6.73	17.06	6.73
Flux under pumping pressure (J_v, L/(m²·h))	13 594		13 598	
Flow velocity (u_v, cm/min)	16.79	6.57	16.79	6.57
retention time (t_{ret}, min)[d]	0.08	0.53	0.08	0.53
$\eta_{NO_3^-}$ (%)[f]	Nil.	5.1 (1.5)[e]	32.0 (3.0)[e]	83.2 (2.7)[e]
$\eta_{SO_4^{2-}}$ (%)[f]	Nil.	5.1 (1.5)[e]	44.3 (2.3)[e]	98.1 (1.5)[e]
$\eta_{PO_4^{3-}}$ (%)[g]	Nil.	14.5 (1.3)[e]	45.3 (6.6)[e]	94.9 (0.6)[e]

Notes: Bed specifications: inside diameter of 23.5 mm cartridge with optimal penetration depth for 100% removal (h) of 1.35 mm (a) and 34.5 mm (b); c, filter loading = 100/bed volume; d, $t_{ret} = h/u_v$; Nil., null, none, or not available; e, standard deviations in parentheses for six measurements; f, nominal feed concentration of 45–50 mg/L (6.8 < pH < 7.0); g, nominal feed concentration of 2.4 mg/L (pH < 12).

from the model poly-GTEAC (Δc_p = 0.350 J/(g·K)), the percentage of grafted polymer could be estimated, resulting in 33% which relatively close to the 29% calculated from the weight gain of 41.39% for QMFC.

3.4. Vapour sorption properties

The moisture sorption behaviour of both the MFC and QMFC was studied to understand the moisture content as a function of the relative humidity (RH) during the adsorption and desorption process. The moisture sorption isotherms (MSIs) were constructed and the data were fitted using the modified GAB model (Viollaz and Rovedo, 1999; Sandoval et al., 2011) (Fig. S3). All fitting parameters can be found in Table S1 together with the parameters obtained using the SSO model. The MFC sample showed the characteristic S-shape (sigmoidal) for lignocellulosic materials with a hysteresis between the desorption and adsorption curves of 1.16, which was lower than that of wood samples (Sánchez -Ferrer et al., 2023). Contrary to that, the QMFC sample showed no hysteresis between the two sorption processes ($\eta \approx 1$), and an enhanced equilibrium moisture content (EMC) of 45% compared to the 20% for MFC at RH of 96% (Fig. 5d). This reversible behaviour and high EMC value were due to the grafting of the amorphous and hydrophilic polymers on the surface of the cellulose crystallites and the free hydroxyl groups of the cellulose amorphous domains. Moreover, the grafting process increased the specific surface area of the quaternised sample from 161 m^2/g (MFC) to 259 m^2/g (QMFC).

Finally, the analysis of the MSI following the SSO model (Willems 2014, 2015) indicates that the bound water moisture capacity ($M_{SSO}{}^0$) in the MFC and QMFC increased from 4.45 mmol/g to 7.90 mmol/g (Table S1) due to the presence of the grafted poly-GTEAC polymer chains (Fig. S4). The value from the QMFC could be assumed to belong entirely to the cationic sites in the poly-GTEAC, since all free hydroxyl groups in MFC should be occupied when working as initiators in the grafting process. Therefore, the number of binding water molecules per repeating unit in the poly-GTEAC chains was 1.5, which could be explained by the presence of one ammonium group and one ether moiety per monomer unit in the polymer backbone.

3.5. Oxoanion removal

The oxoanion removal efficiency was tested using the filter cartridge system and using QMFC and MFC at varying BV and fixed feed loading (100 mL feed per BV). The oxoanion removal performance (η_i) and the process parameters are shown in Table 2. Reported values correspond to three runs with the same filter cartridge. The filter cartridge system has a very high flow rate under pressure. Yet despite low retention time, the removal performance η_i for $NO_3{}^-$, $SO_4{}^{2-}$, and $PO_4{}^{3-}$ are significantly high for the QMFC compared to the MFC, *i.e.*, by 15, 19 and 6 times, respectively. The flux for the MFC and QMFC remains the same, which implies that the GTEAC modification is merely over the fibril surface. Flux can only increase owing to domain expansion within a material, *e.g.*, pore formation or swelling (Pei et al., 2013; Sehaqui et al., 2016; Ahmed and Sánchez-Ferrer, 2025). Though cationic polyelectrolytes grafted onto the surface have much-improved accessibility to interact with the oxoanions, given the contact areas of the fibrils than the wood. The oxoanion removal by MFC is largely due to the uronic groups and carboxylate groups produced during the pulping process (Olszewska et al., 2011). Such retentions are weak and unstable, as evident in Fig. 6b

A higher BV permits a more cross-sectional volume (*i.e.*, ion channels) where the oxoanions can effectively bind with the available ion exchange sites (Tan, 2003; Xia et al., 2008), *i.e.*, cationic polyelectrolyte chains in the QMFC fibres. Greater channel availability enhances mass transfer and ensures more uniform ion distribution throughout the exchanger (Li et al., 2016). To determine the optimum cartridge height, the penetration depth (L_i) for the different oxoanions was estimated for both the QMFC and the MFC as shown in Fig. 6a. The L_i of $NO_3{}^-$, $SO_4{}^{2-}$, and $PO_4{}^{3-}$ for MFC are nearly 34, 75, and 19 times higher than that of QMFC, respectively, which demonstrates the effectiveness of the QMFCs in the oxoanion retention. This also implies that the presence of numerous cationic polyelectrolytes reduces the need for more AEX loading, given its high functionality and capacity to undergo multi-ion exchange. Fig. 6b demonstrates the advantage of using QMFC due to a more stable oxoanion retention over multiple cycles/runs compared to MFC which tends to undergo a leaching effect. At the same time, this also demonstrates a lower requirement to charge/regenerate

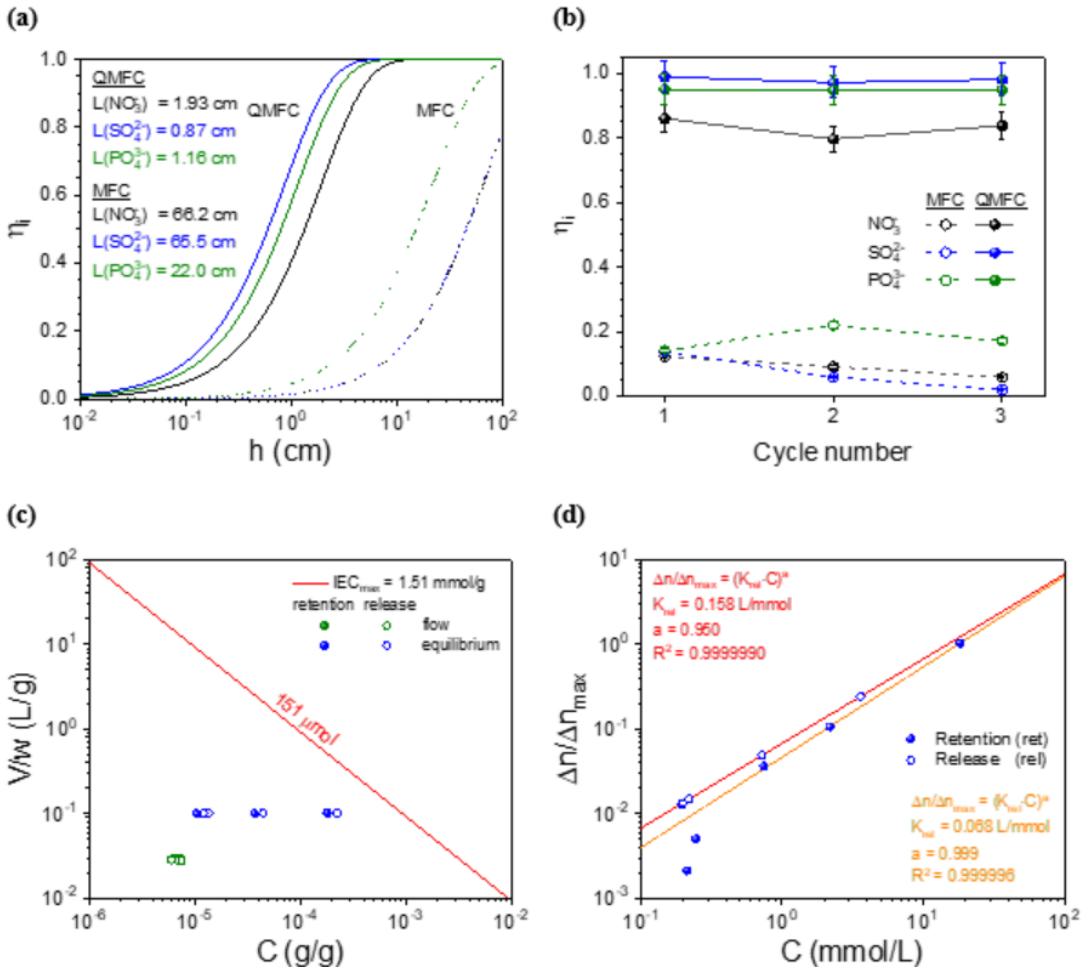

Fig. 6. (a) Log-log plot of h vs. η_i for both the MFC and QMFC sample for the estimation of the optimal penetration depth; (b) Ion exchange stability of MFC and QMFC over repeated cycles; (c) Log-log plot of the mass (w)-normalized head volume (V) vs. NO_3^- concentration (C) retained (ret) and released (rel) for the QMFC fibres (The red line relates to the IEC_{max} of 1.51 mmol/g (*i.e.*, the total number of available sites of 151 μmol $-NEt_3^+$. The green and blue symbols correspond to *IEC* for experiments conducted under flow conditions and equilibrium/zero flow conditions, respectively; (d) Ion exchange isotherms in terms of change in moles number (Δn) of available $-NEt_3^+$ sites at retention time of 48 h under equilibrium for oxoanion retention (filled symbol) and oxoanion release (unfilled symbol) conditions.

the QMFC filter cartridges, and thus can be used multiple times. The removal efficiencies are similar to what has been observed for GTEAC-based quaternised wood membranes (QWMs), *i.e.*, $SO_4^{2-} > PO_4^{3-} > NO_3^-$ (Ahmed and Sánchez-Ferrer, 2025). The binding of SO_4^{2-} to quaternary ammonium (NR_4^+) is well-reported and its hydration effects lead to higher η values than PO_4^{3-}. This order further corresponds to the hydrodynamic radii (R_h) of the oxoanions, as reported by Marcus (1988) and Eiberweiser et al. (2015).

3.6. Polyelectrolytic ion exchange behaviour

The polyelectrolytic behaviour of the QMFC has been studied using the at-equilibrium *IEC* values in dilute and saturated NO_3^- conditions. The *IEC* values were determined in terms of oxoanion retention and release-absorption or desorption, respectively. Fig. 6c shows the breakthrough line in terms of the mass-normalised volume against the total composition of the QMFC fibres. It is evident that for experiments conducted under pressure of 0.2 MPa and high flow of 98.3 mL/min, the *IEC* values were low due to inadequate contact time (0.5 min). Subsequently, for experiments using diluted concentrations at equilibrium under zero flow conditions with t_{ret} of 48 h, the apparent *IEC* values were nearer to the maximum amount needed to go through the IEC_{max} red line (151 μmol $-NEt_3^+$, 1.51 mmol/g). For any value beyond this line, the ion exchanger will be saturated completely and provide lower retentions under static/equilibrium (zero flow) conditions. Alternatively, Figure S5a shows a similar plot between $C_{NO_3^-}$ and V/w_0, and was normalised against the cellulose component or the MFC mass (w_0) used for the synthesis of the corresponding QMFC.

The ion exchange isotherms were plotted in Fig. 6d. The experiments at saturation for both oxoanion retention and release demonstrated the goodness of fit with the Freundlich isotherm with an exponential factor of 0.999 ($R^2 > 0.999996$) and 0.950 ($R^2 > 0.999999$), respectively. Results suggest that a homovalent ion exchange occurred across the multiple available $-NEt_3^+$ groups following a monolayer coverage pattern across the poly-GTEAC chains (Misak, 1993; Azizian and Eris, 2021; Ahmed and

Table 3
Comparison of material properties such as degree of quaternisation (*DQ*), maximum ion exchange (IEC_{max}) or maximum absorption capacity (AC_{max}), and performance parameters such as oxoanion removal efficiencies ($\eta_{NO_3^-}$, $\eta_{SO_4^{2-}}$, and $\eta_{PO_4^{3-}}$) for the QMFC filter cartridge system and other reported cellulosic anionic exchangers.

Item	IEC_{max} (mmol/g)	AC_{max} (mg/g)	t_{ret} (min)	Process flux (L/(m²·h))	Oxoanion removal efficiency			Reference
					$\eta_{NO_3^-}$ (%)	$\eta_{SO_4^{2-}}$ (%)	$\eta_{PO_4^{3-}}$ (%)	
QMFC[a]	1.51[i] 2.13[ii]	94[iii] 132[iii]	0.5	1 3598[iv]	83.2*	98.1*	94.9**	This work
QWM L22[b]	1.07[ii]	63[iv]	30	385–440	84*	98*	89**	Ahmed and Sánchez-Ferrer, 2025
Hardwood Ppy-AC	0.47[iv]	45[iv]	1 440	245	–	82*	–	Hong et al., 2017
BPEI-GTMAC	1.98[iv]	187–192[iv]	1 440	–	58*	43*	–	Gogoi et al., 2019
Peat[c]								
GWP *Kork-deko*[d]	–	1	4 320	63	29–98*	–	–	Escolà Casas et al., 2023
GPC *Kork-deko*[d]		7			4–8*			
CCNF[e]	1.3[i]	801[ii]	11.4	20	80.7*	–	–	Mautner et al., 2017
CCNF[e]	0.6[i]	37[ii]	< 6	6	96*	70*	61*	Sehaqui et al., 2016
Diallylic N^+Me_2 flax[f]	3.4–3.9[i]	208–244[ii]	1 440	1 432	70*	–	–	Maculewicz et al., 2024
Diallylic N^+Me_2	3.6–3.9[i]	226–243[ii]	1 440		69*			
cellulose[g]	3.0–3.5[i]	187–218[ii]	4 320		74*			
AmberLite™ resin[g]								
CCNF	0.25[iii]	25[iii]	75	–	–	80*	–	Muqeet et al., 2017
RS-AE	1.32[iii]	75[iii]	120	–	–	–	80*	Xu et al., 2010

Notes: i, IEC_{max}; ii, degree of quaternisation = $IEC_{0,max}$; iii, $AC = 62 \times IEC$ as NO_3^-; iv, values as SO_4^{2-}; a, cartridge loading 24.7% (*w/V*) QMFC, 14.96 *BV*, bed diameter of 23.5 mm, 0.1 L per batch under nominal pumping pressure of 0.2 MPa; b, membrane grammage 42.9 g/m² in gravity-assisted filtration cell (50 mm diameter); c, bed diameter of 12 mm, 5 L cycle per batch; d, granulated cork pellets (2 mm size, 123 kg/m³) and wetland wood pellets (6–8 mm size, 650 kg/m³), bed diameter of 84 mm, 10 L cycle per batch; nanopaper grammage: e, 30 g/m²; f, placed in permeation cell (1460 mm² area, 0.2 MPa pumping pressure); *, pH feed: 6–7; **, pH feed: < 12.

Sánchez-Ferrer, 2025), which is in agreement with the results obtained from the water sorption isotherms. This, in turn, can lead to non-uniformity and non-homogeneity in the ion-site-specific interactions. The Freundlich behaviour owes to a partial coverage by chemisorption (~50%) on the cationic polyelectrolyte due to double-layer compression effects (Marcus and Hefter, 2006; Wang and Guo, 2020). Ion-pairing (Grothuss hopping) on specific sites of the grafted poly-GTEAC chains can lead to local compressed chains and entanglements that mask other functional groups, *i.e.*, form passive $–NEt_3^+$ sites (Hernández Cifre and de la Torre, 2014).

The ion exchange constants in the case of oxoanion retention and release are given as K_{ret} and K_{rel}, respectively. The release constant for the equilibrium experiments undergoing oxoanion release was significantly low (0.068 L/mmol), *i.e.*, ion exchange is like chemisorption and stable over time (≥ 48 h). Conversely, in the case of oxoanion retention, the ion exchange constant was higher (0.158 L/mmol). This is likely due to lowered double-layer compression under moderate to high NO_3^- concentrations where the multi-functionality of the cationic polyelectrolytes is fully utilized. This has been observed for other surface-immobilised cationic polyelectrolytes based on diallylic-N^+Me_2 copolymers, which can suppress ion transport following polymer layer compressions (Qin et al., 2023). In other words, there is only a small active layer of the poly-GTEAC in low concentrations that caused deviations from expected Freundlich behaviour, and the remnant NEt_3^+ groups were passive in their interactions with the NO_3^-.

The mechanism of this active-passive multi-site ion exchange was visualised in Fig. S1b. This polyelectrolytic behaviour is likely to occur as the exposed $–NEt_3^+$ groups interact with the oxoanions, and the initial units of the poly-GTEAC chain close to the cellulose grafting sites exhibited a lower response (Ahmed and Sánchez-Ferrer, 2025). High oxoanion concentrations under low interference with other oxoanions can mitigate electrostatic repulsion between like-charged ionic groups of the polyelectrolyte, thereby promoting smoother ion mobility (Krishna et al., 2021). The NO_3^- oxoanion had a large hydrodynamic radius (R_h) and lower charge density, which exerted a weaker effect on double-layer compression of the poly-GTEAC chains (Israelachvili, 2011), thus preserving polyelectrolyte functionality and did not lead to *IEC* poisoning or screening effects. The double-layer compression would be more significant under diluted conditions where the imbalance between electrostatic forces could lead to poly-GTEAC chain aggregation and collapse, which would mask/screen $–NEt_3^+$ groups. This explains why the *IEC* value could be low in diluted concentrations despite similar conditions for the equilibrium.

3.7. Comparison of QMFC performance with other cellulosic anionic exchangers

Quaternisation process design: the MFC quaternisation process using the GTEAC offered a simultaneous grafting and polymerisation reaction forming long-chain cationic polyelectrolytes by chain-growth polymerisation, *i.e.*, the poly-GTEAC. The formation of diol-enolic decomposates was prevented owing to the use of anhydrous reaction environments (Ahmed and Sánchez-Ferrer, 2025). Moreover, compared to common quaternisation methods, the proposed method prevented significant cellulose or quaternisation reagent hydrolysis using alkaline systems, *e.g.*, 2.5%–5% (*w/V*) NaOH (Song et al., 2008; Pei et al., 2013; Sehaqui et al., 2016). Moreover, the ion exchange performance for the QMFC was comparable to other cellulosic anion exchangers, as shown in Table 3. However, the QMFC holds the advantage of achieving total ion exchange for a lower retention time (t_{ret}) of 0.5 min in contrast to the other systems. This was attributed to the higher GTEAC degree of polymerisation in MFCs, which yielded multi-functional ion ex-

change sites allowing for rapid *IEC*. This offers a method of surface modification that can yield high *IEC* or high AC exchangers, which can perform efficiently at lower operating times. Furthermore, the QMFC preparation process is not concerned with the challenges associated with substrate homogenisation to prepare quaternary anion exchangers.

Performance assessment and technoeconomics: As shown in Table 3, residence time for the QMFC filter cartridge system was low under the pumped flow (*i.e.*, 0.5 min), though offering high oxoanion removal/retention (η). The QMFC filter cartridge offered improved *IEC* or *AC* performance in contrast to other cellulosic or lignocellulosic anion exchangers. The use of sustainable, renewable materials, *e.g.*, cellulose together with a *DQ* process, such as the one proposed herein, can yield effective ion exchange/ultrafiltration systems. These systems can be used for ultra-deionised water production for lab or technical use, as guard filtration systems, and as portable filtration devices to obtain safe drinking water, as performed herein. The results indicate that the QMFC can decrease the NO_3^-, SO_4^{2-}, and PO_4^{3-} concentration to World Health Organization recommends acceptable levels as <11 mg/L, <250 mg/L, and <0.2 mg/L from polluted or contaminated water. The process economics are also better realised by the cost-effectiveness of the GTEAC quaternisation, which QMFC costs 3.5 yuan (euro dollar)/kg, inclusive of energy and material inputs which is 10 times lower than commercial AmberLite^{TM} resins of 254–340 yuan (euro dollar)/kg.

Process sustainability, safety and energy efficiency: Process sustainability, safety and energy efficiency have been quantified using selected parameters based on the process-specific Green Chemistry Metrics reported by DeVierno Kreuder et al. (2017). The quaternisation process leads to a two-third decomposition of the original GTEAC (Ahmed and Sánchez-Ferrer, 2025). The process mass efficiency (*PME*) was calculated as 2.79 and the *E*-factor was 1.97, the latter corresponding to the recommended values for bulk chemicals, *i.e.*, < 1–5 (Sheldon, 2007, 2018). The values imply adequate resource utilization and that the waste production is low and utilized in the process. The low-hazard chemical synthesis (*HCS*) score is 339.7, which indicates a quaternisation process design with minimal safety risk compared to conventional organic methods which can have *HCS* higher than 10^3 (DeVierno Kreuder et al., 2017). The energy efficiency (*EE*) score amounts to 66.3, corresponding to less energy-intensive modification processes operating at or near the boiling point of water at near-ambient pressure, and lower *EE* values correspond to high energy wastage.

4. Conclusions

Microfibrillated cellulose (MFC) fibres were functionalized by an *in-situ* graft chain-growth polymerisation reaction using the reactive ionic liquid (RIL) glycidyltriethylammonium chloride (GTEAC). This method also avoided the use of harsh alkaline conditions typically employed in cellulose modification (Song et al., 2008; Pei et al., 2013; Sehaqui et al., 2016; Mautner et al., 2017), reducing waste generation and ensuring minimal degradation of cellulose fibres. These metrics confirmed the process as resource-efficient, environmentally benign, and economically viable. The resulting QMFC had a total number of $–NEt_3^+$ groups equal to 2.13 mmol/g (151 μmol $–NEt_3^+$ sites relative to the poly-GTEAC component).

Structural characterisation using SEM/EDX and WAXS/SAXS confirmed that the grafting predominantly occurred on the surface of the cellulose crystallites and in the amorphous regions of cellulose, preserving the cellulose I monoclinic structure. The WAXS analysis showed retention of the crystalline lattice parameters, ensuring the stability of the underlying cellulose framework while decreasing the degree of crystallinity of the sample from 85% to 56% due to the presence of the amorphous poly-GTEAC. The SAXS analysis revealed an increase in lateral spacing of 35% due to the incorporation of amorphous polyelectrolytic grafts. Thermal characterisation revealed an apparent decrease in the decomposition temperature of MFC from 355 °C to 340 °C (QMFC). The grafted poly-GTEAC lowered decomposition temperature owing to its high amorphous content, *i.e.*, chain mobility in the swollen state.

The formation of cationic polyelectrolytes through *in-situ* polymerisation of GTEAC resulted in multi-site ion exchange interactions and enhanced hydrophilicity, which in turn improved oxoanion accessibility in hydrated conditions. The QMFC achieved an IEC_{max} of 1.51 mmol/g and demonstrated competitive oxoanion removal efficiencies under flow conditions, achieving 83.2%, 98.1%, and 94.9% for NO_3^-, SO_4^{2-}, and PO_4^{3-}, respectively. Furthermore, the QMFC maintained its performance over multiple filtration cycles, implying performance stability and reusability. A Freundlich behaviour was observed for the QMFCs, indicating multi-layer ion-site interactions, with exponential factor values of 0.950–0.999, and oxoanion exchange constants K_{rel} of 0.068 L/mmol and K_{ret} of 0.158 L/mmol, owing to the presence of numerous cationic polyelectrolytic sites.

Compared to traditional cellulosic anion exchangers, the QMFC outperformed in terms of *IEC* (or the *AC*) and removal efficiencies, benefiting from the inclusion of long-chain cationic polyelectrolytes. The quaternization process adhered to green chemistry principles (DeVierno Kreuder et al., 2017), as reflected by its process mass efficiency of 2.79, an *E*-factor of 1.97, and an energy efficiency score of 66.3. The scalability of the process, combined with the material's low-cost preparation (3.5 yuan (euro dollar)/kg), further emphasized its potential for industrial-scale applications. These properties positioned QMFC as a sustainable alternative for water purification systems, particularly for the removal of anionic pollutants such as nitrates, sulphates, and phosphates. Future studies are likely to focus on the optimization of grafting parameters, feasibility scale-up, and material integration into commercial filtration systems. Additionally, *IEC*/absorption studies with organic anionic pollutants, such as dyes and perfluoroalkylsulphonate contaminants removed by QMFC, would further enhance its versatility.

Availability of data

Data has been disclosed herein in its entirety and is available upon request.

Declaration of competing interest

The authors declare that they have no known competing financial interests or personal relationships that could have appeared to influence the work reported in this paper.

CRediT authorship contribution statement

Muzamil Jalil Ahmed: Conceptualization, Data curation, Formal analysis, Funding acquisition, Investigation, Methodology, Visualization, Writing – original draft. **Baohu Wu:** Investigation, Writing – original draft. **Antoni Sánchez-Ferrer:** Conceptualization, Data curation, Formal analysis, Investigation, Methodology, Visualization, Writing – original draft, Project administration, Resources, Software, Supervision, Validation, Writing – review & editing.

Acknowledgements

Muzamil Jalil Ahmed acknowledges the support received from the Deutscher Akademische Austauchsdienst (DAAD) in the form of the Short-term Research (No. 57693450) that partially funded his research stay at the time of this research. Muzamil Jalil Ahmed further acknowledges the technical support received from the technical staff of the Bayerische NMR Zentrum (BNMRZ) of the Department of Chemistry at the Technical University of Munich. The authors will further extend their gratitude to Anja Vieler from the Microscopy Lab at the Wood Research Institute (HFM) for her technical assistance with the SEM/EDX characterisation.

Supplementary materials

References

Ahmed, M.J., Ashfaq, J., Sohail, Z., Channa, I.A., Sánchez-Ferrer, A., Ali, S.N., Chandio, A.D., 2024. Lignocellulosic bioplastics in sustainable packaging–Recent developments in materials design and processing: a comprehensive review. Sustain. Mater. Technol. 41, e01077.

Ahmed, M.J., Sánchez-Ferrer, A., 2025. Wood-supported cationic polyelectrolyte membranes from a reactive ionic liquid for water detoxification. Chem. Eng. J. 505, 158841.

Anastas, P.T., Warner, J.C., 2000. Green Chemistry: Theory and Practice. Oxford University Press, New York, p. 30.

Arcari, M., Zuccarella, E., Axelrod, R., Adamcik, J., Sánchez-Ferrer, A., Mezzenga, R., et al., 2019. Nanostructural properties and twist periodicity of cellulose nanofibrils with variable charge density. Biomacromolecules 20, 1288–1296.

Azizian, S., Eris, S., 2021. Adsorption isotherms and kinetics. In: Ghaedi, M. (Ed.), Interface Science and Technology. Elsevier, Amsterdam, pp. 445–509.

Berthold, J., Rinaudo, M., Salmeń, L., 1996. Association of water to polar groups; estimations by an adsorption model for ligno-cellulosic materials. Colloids Surf. A Physicochem. Eng. Aspects 112, 117–129.

Bertsch, P., Sánchez-Ferrer, A., Bagnani, M., Isabettini, S., Kohlbrecher, J., Mezzenga, R., et al., 2019. Ion-induced formation of nanocrystalline cellulose colloidal glasses containing nematic domains. Langmuir 35, 4117–4124.

Brodin, M., Vallejos, M., Opedal, M.T., Area, M.C., Chinga-Carrasco, G., 2017. Lignocellulosics as sustainable resources for production of bioplastics–A review. J. Clean. Prod. 162, 646–664.

Cheng, X., Wang, J.C., Liao, Y.C., Li, C.P., Wei, Z.D., 2018. Enhanced conductivity of anion-exchange membrane by incorporation of quaternized cellulose nanocrystal. ACS Appl. Mater. Interfaces 10, 23774–23782.

DeVierno Kreuder, A., House-Knight, T., Whitford, J., Ponnusamy, E., Miller, P., Jesse, N., et al., 2017. A method for assessing greener alternatives between chemical products following the 12 principles of green chemistry. ACS Sustainable Chem. Eng. 5, 2927–2935.

Eftekhari, A., Saito, T., 2017. Synthesis and properties of polymerized ionic liquids. Eur. Polym. J. 90, 245–272.

Eiberweiser, A., Nazet, A., Hefter, G., Buchner, R., 2015. Ion hydration and association in aqueous potassium phosphate solutions. J. Phys. Chem. B 119, 5270–5281.

Engelhardt, M., Gilg, H.A., Richter, K., Sanchez-Ferrer, A., 2024. Adhesion-related properties of silver birch (*Betula* Pendula Roth) wood as affected by hydrophilic extraction. Wood Sci. Technol. 58, 379–402.

Escolà Casas, M., Guivernau, M., Viñas, M., Fernández, B., Cáceres, R., Biel, C., et al., 2023. Use of wood and cork in biofilters for the simultaneous removal of nitrates and pesticides from groundwater. Chemosphere 313, 137502.

Fida, M., Li, P.Y., Wang, Y.H., Khorshed Alam, S.M., Nsabimana, A., 2022. Water contamination and human health risks in Pakistan: a review. Expo. Health 15, 619–639.

Gogoi, H., Leiviskä, T., Rämö, J., Tanskanen, J., 2019. Production of aminated peat from branched polyethylenimine and glycidyltrimethylammonium chloride for sulphate removal from mining water. Environ. Res. 175, 323–334.

Gupta, P.K., Uniyal, V., Naithani, S., 2013. Polymorphic transformation of cellulose I to cellulose II by alkali pretreatment and urea as an additive. Carbohydr. Polym. 94, 843–849.

Hassan, M.L., 2006. Quaternization and anion exchange capacity of Sponge Gourd (*Luffa cylindrica*). J. Appl. Polym. Sci. 101, 2495–2503.

Hernández Cifre, J.G., de la Torre, J.G., 2014. Ionic strength effect in polyelectrolyte dilute solutions within the Debye–Hückel approximation: monte Carlo and Brownian dynamics simulations. Polym. Bull. 71, 2269–2285.

Hong, S.Q., Cannon, F.S., Hou, P., Byrne, T., Nieto-Delgado, C., 2017. Adsorptive removal of sulfate from acid mine drainage by polypyrrole modified activated carbons: effects of polypyrrole deposition protocols and activated carbon source. Chemosphere 184, 429–437.

Huang, K.H., Maltais, A., Liu, J.X., Wang, Y.X., 2022. Wood cellulose films regenerated from NaOH/urea aqueous solution and treated by hot pressing for food packaging application. Food Biosci 50, 102177.

Israelachvili, J.N., 2011. Electrostatic forces between surfaces in liquids. In: Intermolecular and Surface Forces. Elsevier, Amsterdam, pp. 291–340.

Jakubovic, A.O., Brook, B.N., 1961. Anion exchangers based on cellulose: I. preparation and general properties. Polymer (Guildf) 2, 18–26.

Koga, Y., Sebe, F., Nishikawa, K., 2013. Effects of tetramethyl- and tetraethylammonium chloride on H_2O: calorimetric and near-infrared spectroscopic study. J. Phys. Chem. B 117, 877–883.

Kono, H., 2017. Cationic flocculants derived from native cellulose: preparation, biodegradability, and removal of dyes in aqueous solution. Resour. Effic. Technol. 3, 55–63.

Kopač, T., Krajnc, M., Ručigaj, A., 2022. A rheological study of cationic micro- and nanofibrillated cellulose: quaternization reaction optimization and fibril characteristic effects. Cellulose 29, 1435–1450.

Krishna, B.A., Lindhoud, S., de Vos, W.M., 2021. Hot-pressed polyelectrolyte complexes as novel alkaline stable monovalent-ion selective anion exchange membranes. J. Colloid Interface Sci. 593, 11–20.
Lavoine, N., Desloges, I., Dufresne, A., Bras, J., 2012. Microfibrillated cellulose: its barrier properties and applications in cellulosic materials: a review. Carbohydr. Polym. 90, 735–764.
Li, H., Guo, R., Tian, X., Fan, Y.B., Wang, C.Y., Huan, S.Q., 2024. Preparation of lignin/nanocellulose hybrid particles by co-precipitation method. Journal of Forestry Engineering 9, 107–114.
Li, H.C., Shan, C., Zhang, Y.Y., Cai, J.G., Zhang, W.M., Pan, B.C., 2016. Arsenate adsorption by *hydrous* ferric oxide nanoparticles embedded in cross-linked anion exchanger: effect of the host pore structure. ACS Appl. Mater. Interfaces 8, 3012–3020.
Lu, Y.C., He, Q., Fan, G.Z., Cheng, Q.P., Song, G.S., 2021. Extraction and modification of hemicellulose from lignocellulosic biomass: a review. Green Process. Synth. 10, 779–804.
Maculewicz, J., O'Sullivan, A.D., Barker, D., Wai, K.T., Basharat, S., Bello-Mendoza, R., 2024. Novel quaternary ammonium functionalized cellulosic materials for nitrate adsorption from polluted waters. Water Air Soil Pollut 236, 47.
Marcus, Y., 1988. Ionic radii in aqueous solutions. Chem. Rev. 88, 1475–1498.
Marcus, Y., Hefter, G., 2006. Ion pairing. Chem. Rev. 106, 4585–4621.
Marković-Nikolić, D.Z., Bojić, A.L., Savić, S.R., Petrović, S.M., Cvetković, D.J., Cakić, M.D., et al., 2018. Synthesis and physicochemical characterization of anion exchanger based on green modified bottle gourd shell. J. Spectrosc. 2018, 1–16.
Mautner, A., Kobkeatthawin, T., Bismarck, A., 2017. Efficient continuous removal of nitrates from water with cationic cellulose nanopaper membranes. Resour. Effic. Technol. 3, 22–28.
McClure, J.D., 1970. Glycidyltrimethylammonium chloride and related compounds. J. Org. Chem. 35, 2059–2061.
Misak, N.Z., 1993. Langmuir isotherm and its application in ion-exchange reactions. React. Polym. 21, 53–64.
Muqeet, M., Malik, H., Mahar, R.B., Ahmed, F., Khatri, Z., Carlson, K., 2017. Cationization of cellulose nanofibers for the removal of sulfate ions from aqueous solutions. Ind. Eng. Chem. Res. 56, 14078–14088.
Olszewska, A., Eronen, P., Johansson, L.S., Malho, J.M., Ankerfors, M., Lindström, T., et al., 2011. The behaviour of cationic nanofibrillar cellulose in aqueous media. Cellulose 18, 1213–1226.
Pei, A.H., Butchosa, N., Berglund, L.A., Zhou, Q., 2013. Surface quaternized cellulose nanofibrils with high water absorbency and adsorption capacity for anionic dyes. Soft Matter 9, 2047–2055.
Qin, H.G., Du, Y.F., Bai, Y.Y., Li, F.Z., Yue, X., Wang, H., et al., 2023. Surface-immobilized cross-linked cationic polyelectrolyte enables CO_2 reduction with metal cation-free acidic electrolyte. Nat. Commun. 14, 5640.
Sánchez-Ferrer, A., Engelhardt, M., 2025. Determination of the water diffusivity dependence with the flow rate using a DVS equipment. Eur. J. Wood Wood Prod. 83, 24.
Sánchez-Ferrer, A., Engelhardt, M., Richter, K., 2023. Anisotropic wood–water interactions determined by gravimetric vapor sorption experiments. Cellulose 30, 3869–3885.
Sandoval, A.J., Barreiro, J.A., Müller, A.J., 2011. Determination of moisture adsorption isotherms of rice flour using a dynamic vapor sorption technique. Interciencia 36, 848–852.
Sata, T., 2004. Ion Exchange membranes: preparation, characterization, modification and application. Royal Society of Chemistry, Cambridge.
Scheuchzer, P., Zimmerman, M.B., Zeder, C., Sánchez-Ferrer, A., Moretti, D., 2022. Higher extrusion temperature induces greater formation of less digestible type V and retrograded starch in iron-fortified rice grains but does not affect iron bioavailability: stable isotope studies in young women. J. Nutr. 152, 1220–1227.
Schmitt, F., Granet, R., Sarrazin, C., MacKenzie, G., Krausz, P., 2011. Synthesis of anion exchange membranes from cellulose: crosslinking with diiodobutane. Carbohydr. Polym. 86, 362–366.
Sehaqui, H., Mautner, A., Perez de Larraya, U., Pfenninger, N., Tingaut, P., Zimmermann, T., 2016. Cationic cellulose nanofibers from waste pulp residues and their nitrate, fluoride, sulphate and phosphate adsorption properties. Carbohydr. Polym. 135, 334–340.
Shao, X.Y., Wang, J., Yao, X.J., Wang, Y.B., Song, W.B., Xu, D.H., et al., 2024. Cellulose based hierarchically structured anion-exchange fiber for efficient dye adsorption. Cellulose 31, 411–426.
Sheldon, R.A., 2007. The E factor: fifteen years on. Green Chem. 9, 1273–1283.
Sheldon, R.A., 2018. Metrics of green chemistry and sustainability: past, present, and future. ACS Sustainable Chem. Eng. 6, 32–48.
Song, Y.B., Sun, Y.X., Zhang, X.Z., Zhou, J.P., Zhang, L.N., 2008. Homogeneous quaternization of cellulose in NaOH/urea aqueous solutions as gene carriers. Biomacromolecules 9, 2259–2264.
Tan, H.K.S., 2003. Ion exchange accompanied by neutralization in an anion bed. Chem. Eng. J. 91, 59–66.
Viollaz, P.E., Rovedo, C.O., 1999. Equilibrium sorption isotherms and thermodynamic properties of starch and gluten. J. Food Eng. 40, 287–292.
Wang, J.L., Guo, X., 2020. Adsorption isotherm models: classification, physical meaning, application and solving method. Chemosphere 258, 127279.
Waseem, A., Arshad, J., Iqbal, F., Sajjad, A., Mehmood, Z., Murtaza, G., 2014. Pollution status of Pakistan: a retrospective review on heavy metal contamination of water, soil, and vegetables. Biomed Res. Int. 2014, 813206.
Willems, W., 2014. The water vapor sorption mechanism and its hysteresis in wood: the water/void mixture postulate. Wood Sci. Technol. 48, 499–518.
Willems, W., 2015. A critical review of the multilayer sorption models and comparison with the sorption site occupancy (SSO) model for wood moisture sorption isotherm analysis. Holzforschung 69, 67–75.
Wu, F., Misra, M., Mohanty, A.K., 2021. Challenges and new opportunities on barrier performance of biodegradable polymers for sustainable packaging. Prog. Polym. Sci. 117, 101395.
Xia, H.F., Lin, D.Q., Yao, S.J., 2008. Chromatographic performance of macroporous cellulose-tungsten carbide composite beads as anion-exchanger for expanded bed adsorption at high fluid velocity. J. Chromatogr. A 1195, 60–66.
Xu, X., Gao, B.Y., Yue, Q.Y., Zhong, Q.Q., Zhan, X., 2010. Preparation, characterization of wheat residue based anion exchangers and its utilization for the phosphate removal from aqueous solution. Carbohydr. Polym. 82, 1212–1218.
Xue, Z.M., Yan, H.L., 2024. Advances on lignocellulose pretreatment by choline chloride-based deep eutectic solvents. J. Forest. Engineer. 9, 32–44.